Universiteit Leiden
The Netherlands

Electrocatalytic CO2 reduction toward liquid fuels : on heterogeneous electrocatalysts and heterogenized molecular catalysts

Birdja, Y.Y.

Citation

Birdja, Y. Y. (2018, April 19). *Electrocatalytic CO2 reduction toward liquid fuels : on heterogeneous electrocatalysts and heterogenized molecular catalysts*. Retrieved from https://hdl.handle.net/1887/61513

Version:	Not Applicable (or Unknown)
License:	Licence agreement concerning inclusion of doctoral thesis in the Institutional Repository of the University of Leiden
Downloaded from:	https://hdl.handle.net/1887/61513

Note: To cite this publication please use the final published version (if applicable).

Cover Page

Universiteit Leiden

Leiden University Repository

The handle http://hdl.handle.net/1887/61513 holds various files of this Leiden University dissertation

Author: Birdja, Yuvraj Y.
Title: Electrocatalytic CO2 reduction toward liquid fuels : on heterogeneous electrocatalysts and heterogenized molecular catalysts
Date: 2018-04-19

APPENDIX B

Supporting Information to Chapter 5

Influence of the Metal center of Metalloprotoporphyrins on the Electrocatalytic CO_2 reduction to Formic acid

B.1 Blank voltammograms

Before each experiment, the immobilization of the MPP is qualitatively verified by measuring a cyclic voltammogram in the potential range of -0.5 and 1.3 V_{RHE} before and after immobilization. The presence of additional redox waves ensures the immobilization of the MPP. In Figure B.1 the voltammograms for RhPP, InPP and SnPP are shown. It can be seen that PG itself already shows redox peaks (between 0.5-0.7 V) and a reduction peak (around -0.3 V). These peaks are ascribed to electron transfer processes of surface functional groups on PG as studied extensively by Compton and coworkers.[1–4] The extra peaks which become visible after immobilization of the MPP are associated to redox transitions of the metal center itself. The exact nature of the redox transition is not investigated herein as only a qualitative proof of immobilization is desired.

In Figure B.2a the formation of volatile products on pristine PG in $HClO_4$, pH = 3 is depicted. As can be seen only H_2 is produced on PG. In Figure B.2b the CO_2 reduction on pristine PG is measured and again only significant amounts of H_2 are observed. As the m/z = 44 and m/z = 28 signals decrease at negative potentials it is assumed that CO_2 is consumed at these potentials (CO follows the CO_2 signal, unless the signal is much higher compared to CO_2). As no other mass signals were found to increase it is likely that CO_2 reduction on PG does not produce significant amounts of products and the current is mainly due to HER. The CO_2 consumption at negative potentials is ascribed to an increase in local pH at the electrode surface, converting CO_2 into HCO_3^-.

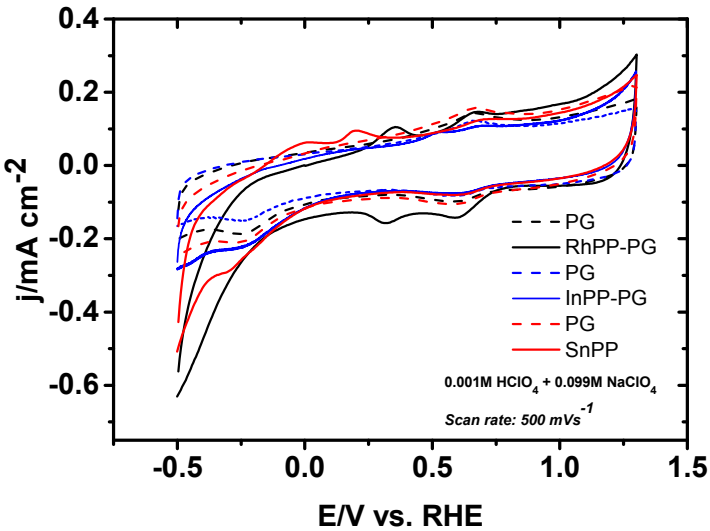

Figure B.1 Blank CV's on (immobilized MPPs on) PG in 0.001 M $HClO_4$ + 0.099 M $NaClO_4$. Scan rate: 500 mV s^{-1}.

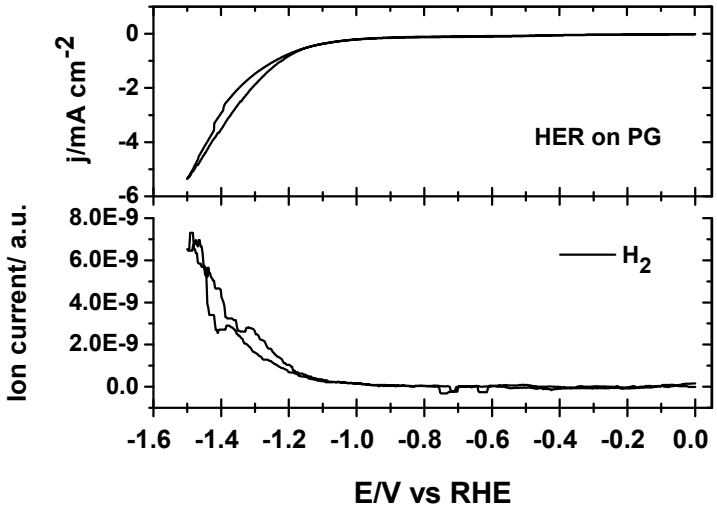

(a)

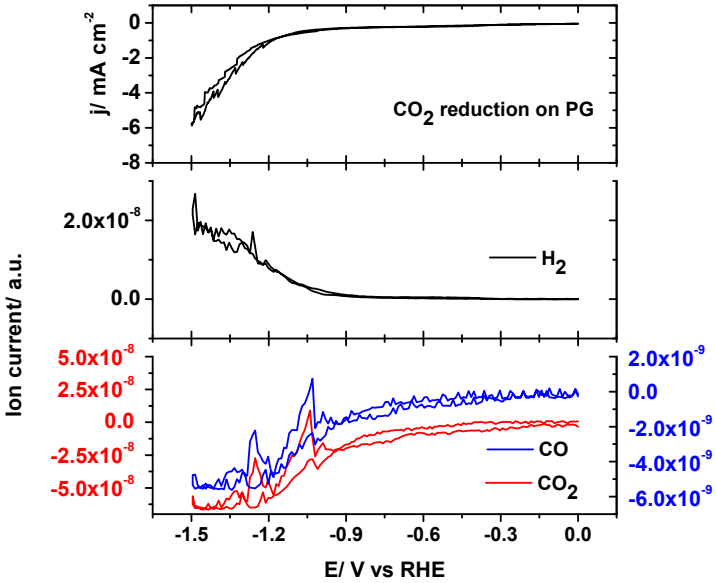

(b)

Figure B.2 HER (a) and CO_2 reduction (b) on pristine pyrolytic graphite in 0.001 M $HClO_4$ + 0.099 M $NaClO_4$. Scan rate 1 mV s^{-1}.

B.2 IR compensation

In this work the electrolysis experiments were IR corrected by the potentiostat's IR compensation function, while voltammetric experiments on the 10 mm diameter PG electrode were corrected mathematically afterwards. For the latter experiments, the voltammograms sometimes show unrealistic behavior (more than one datapoint corresponding to a single potential) which is caused by the combination of current fluctuations at negative potentials (H_2 bubbles) and IR correction after the measurement. Before each electrolysis experiment the uncompensated resistance was determined by potentiostatic electrochemical impedance spectroscopy (Iviumstat or Compactstat, Ivium Technologies) on the pristine PG electrode in the blank electrolyte at E = 0.2 V_{RHE} which is a potential within the doublelayer region. The frequency range was usually between 20 kHz and 10 Hz. In a ideal system the limiting case of inifinite frequency would lead to the uncompensated resistance. In the Nyquist plot, a line is fitted through the datapoints corresponding to higher frequencies and the intercept with the real axis is obtained. To avoid overcompensation and instabilities in the potentiostat control, 85% of this value is used in the potentiostat's IR compensation function. An example of a typical Nyquist plot for a PG electrode is shown in Figure B.3. In table B.1 the used electrolytes are shown together with their solution resistance in the one-compartment electrochemical cell.

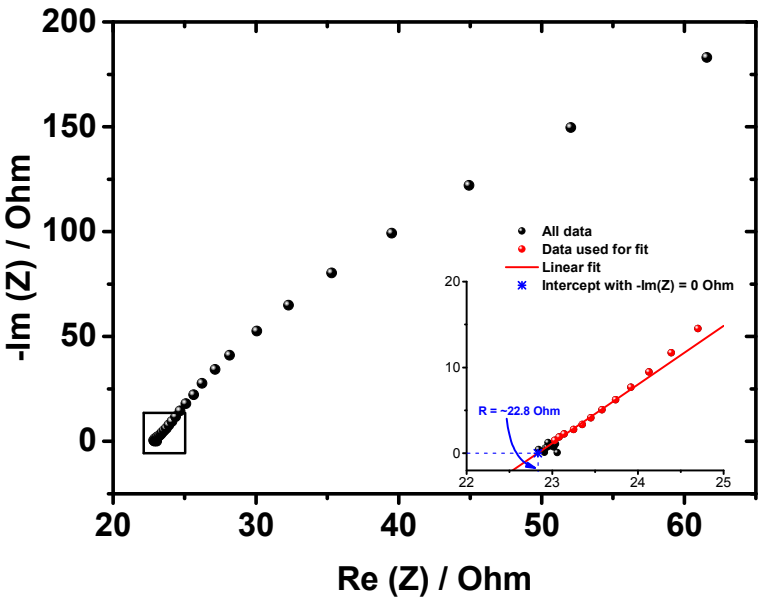

Figure B.3 Example of Nyguist plot from which the cell resistance is derived

Table B.1 Composition of the used electrolytes and their solution resistance

pH	Electrolyte solution			Resistance
1	0.1 M $HClO_4$			≈ 19.8 Ω
3	0.001 M $HClO_4$	+	0.099M $NaClO_4$	≈ 71.1 Ω
4.0-4.1	0.001 M H_3PO_4	+	0.1 M KH_2PO_4	≈ 82.2 Ω
5.8	0.1 M KH_2PO_4	+	0.01 M K_2HPO_4	≈ 59.7 Ω
6.8	0.1 M KH_2PO_4	+	0.1 M K_2HPO_4	≈ 27.2 Ω
7.8	0.01 M KH_2PO_4	+	0.1 M K_2HPO_4	≈ 37.9 Ω
9.6-9.8	0.1 M K_2HPO_4	+	0.001 M K_3PO_4	≈ 38.7 Ω
11.6	0.1 M K_2HPO_4	+	0.1 M K_3PO_4	≈ 17.9 Ω

B.3 OLEMS on different MPPs

In this section the OLEMS results for CO_2 reduction on the different MPPs are shown, indicating the volatile products that have been formed. Formation of CO is hard to see, since the CO signal (m/z = 28) follows the CO_2 (m/z = 44) signal due to fragmentation of CO_2 in the mass chamber. CO can be detected when large amounts are produced as seen for NiPP. For the HCOOH producing porphyrins (RhPP, SnPP and InPP), we confirmed the absence of CO production with gas chromatography.

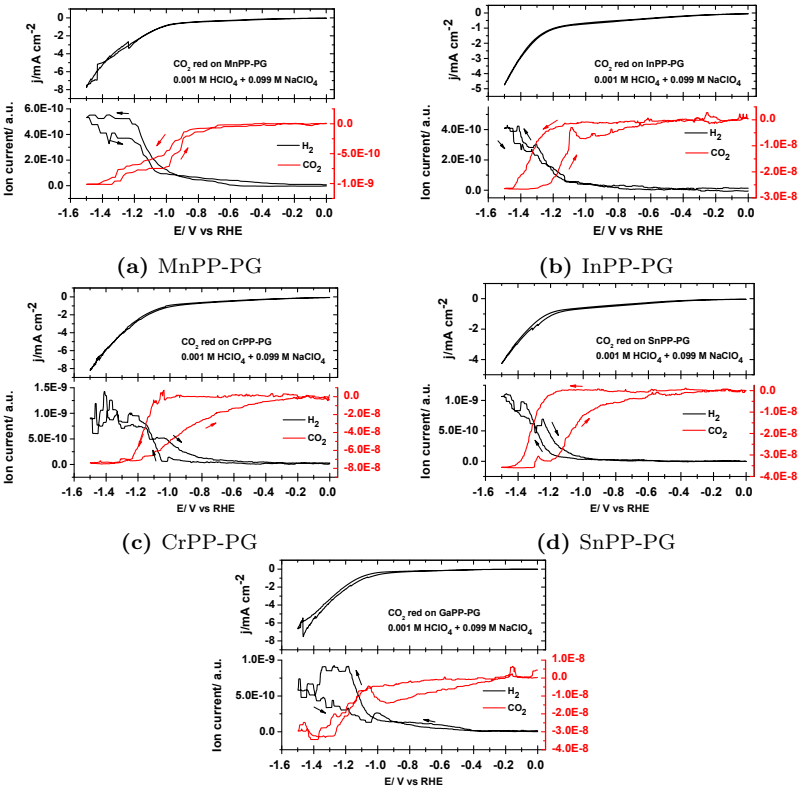

(a) MnPP-PG **(b)** InPP-PG

(c) CrPP-PG **(d)** SnPP-PG

(e) GaPP-PG

Figure B.4 OLEMS results during CO_2 reduction on different MPPs in 0.001 M $HClO_4$ + 0.099 M $NaClO_4$. Scan rate: 1 mV s^{-1}.

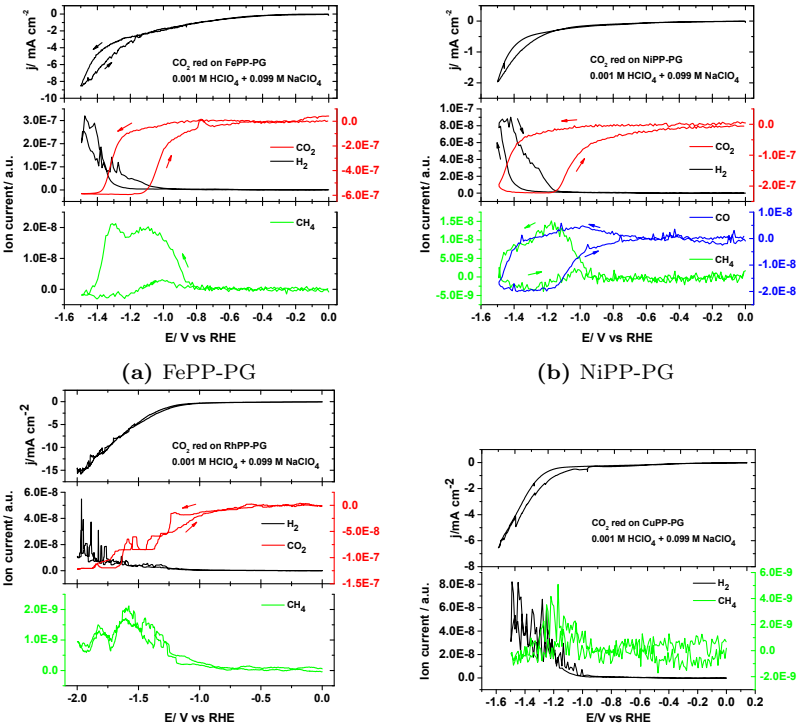

(a) FePP-PG **(b)** NiPP-PG

(c) RhPP-PG **(d)** CuPP-PG

Figure B.5 OLEMS results during CO_2 reduction on different MPPs in 0.001 M $HClO_4$ + 0.099 M $NaClO_4$. Scan rate: 1 mV s^{-1}.

B.4 Normalized concentration profiles

The graphs shown in Figures 5.7a, 5.8a and 5.9a are normalized by the maximum concentration and shown in Figure B.6 to show the shift of the concentration profiles of RhPP with pH. This shift is less prominent for InPP and SnPP.

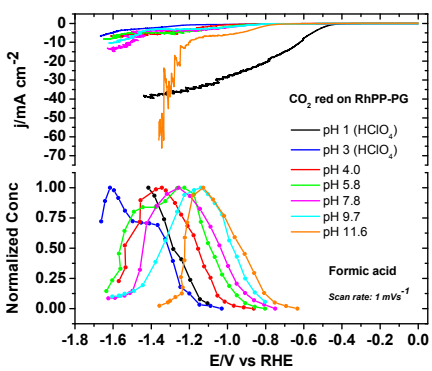

(a) RhPP

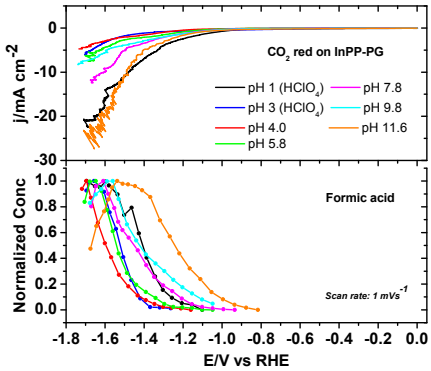

(b) InPP

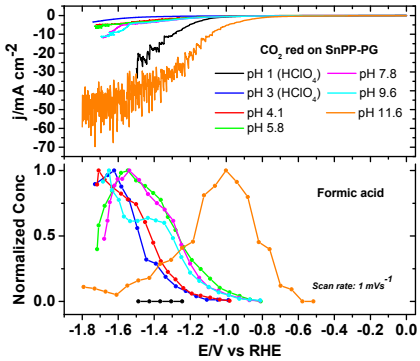

(c) SnPP

Figure B.6 CO_2 reduction on formic acid producing MPP at different pH's

B.5 Comparison definition of onset potential

As the definition of the onset potential is somewhat arbitrary, a different definition could lead to different results. However, in Figure B.7 it is shown that for both, the concentration profile and the current profile, the trend of the onset potential as a function of pH is the same irrespective of the method used. The onset potentials shown in Figure 5.10 are based on an average of different definitions.

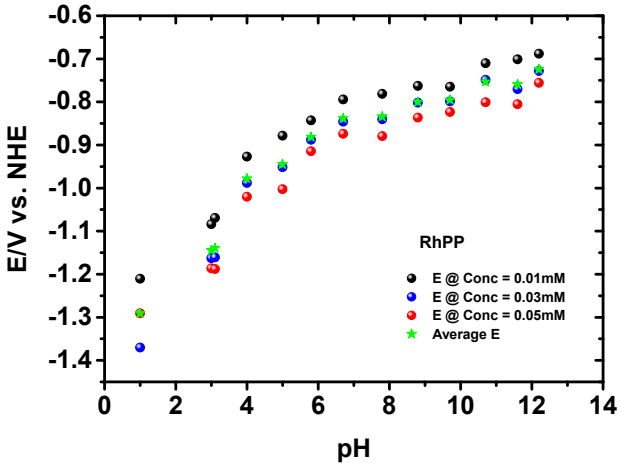

(a) Onset potential of concentration profile

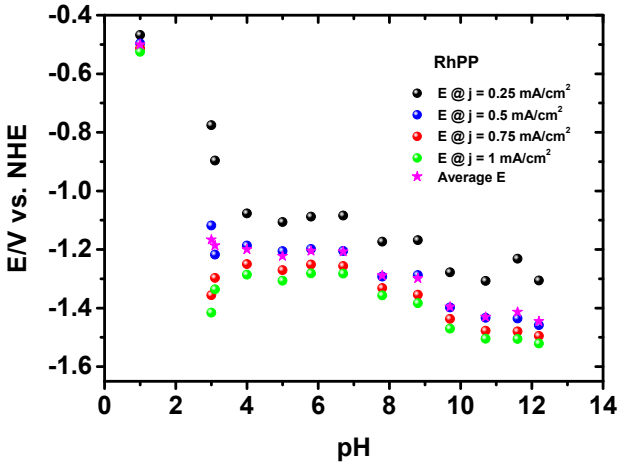

(b) Onset potential of current profile

Figure B.7 Comparison of different definitions of the onset potentials

B.6 Faradaic efficiency

The faradaic efficiencies determined for RhPP, InPP and SnPP in different electrolytes at a potential of E = -1.5 V_{RHE}.

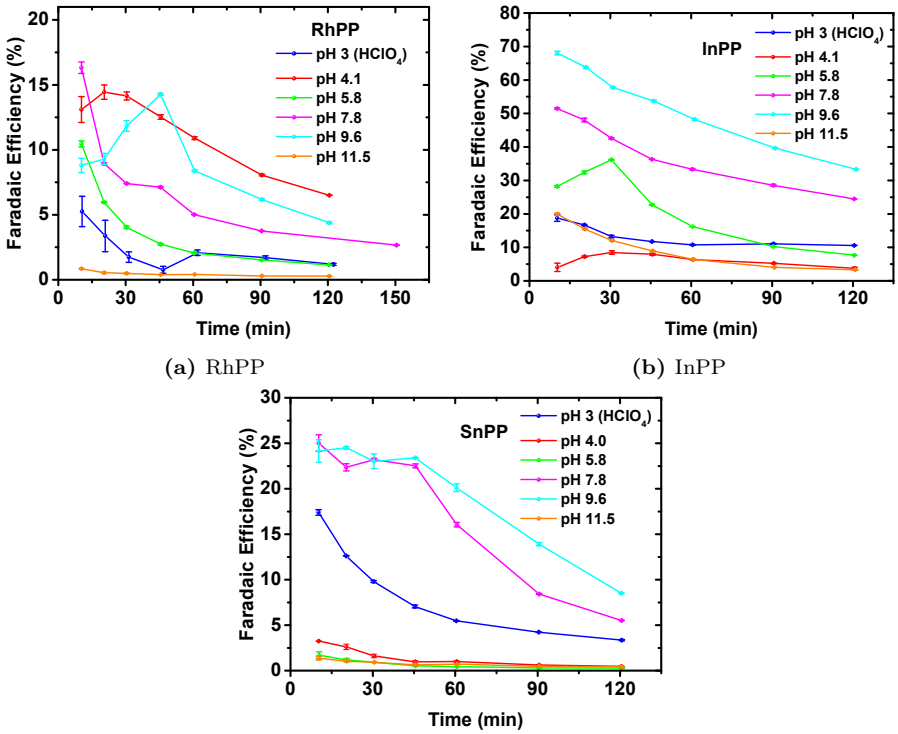

(a) RhPP **(b)** InPP

(c) SnPP

Figure B.8 Faradaic efficiencies in different electrolytes at E = -1.5V versus time

B.7 Deactivation of the catalyst

The deactivation of the catalyst is looked into by comparing the blank voltammograms of the immobilized porphyrins before and after the HER or CO_2 reduction as shown in Figure B.9. It can be seen that the porphyrin-specific redox peaks have disappeared after HER and CO_2 reduction. As this observation is found for all the different MPPs and for both, HER and CO_2 reduction, the deactivation is believed to be associated to the destruction of the porphyrin structure or immobilization of the porphyrin on PG as a result of the very negative potentials.

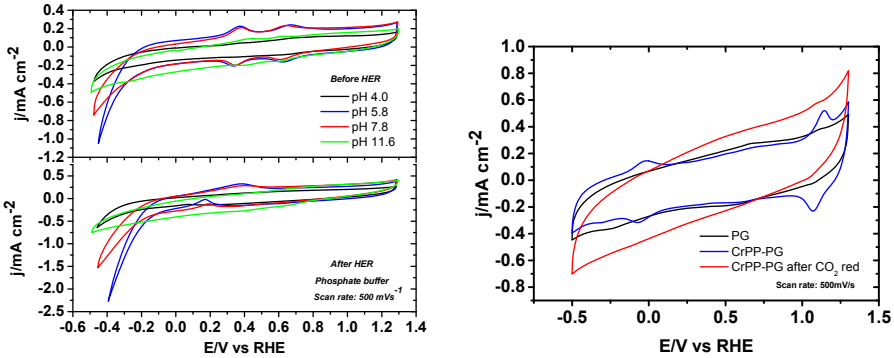

(a) (b)

Figure B.9 Blank voltammograms before and after (a) HER on immobilized RhPP in different phosphate buffers and (b) CO_2 reduction on immobilized CrPP in 0.001 M $HClO_4$ + 0.099 M $NaClO_4$

B.8 Influence of the buffer capacity

The buffer capacity may have an influence on the catalytic activity as it affects the local pH during CO_2 reduction. As shown in Figure B.10, a higher buffer capacity leads to a higher current. The formation of formic acid is also dependent on the buffer capacity. These results may indicate that the local pH may play a role in the catalytic activity of the immobilized porphyrins.

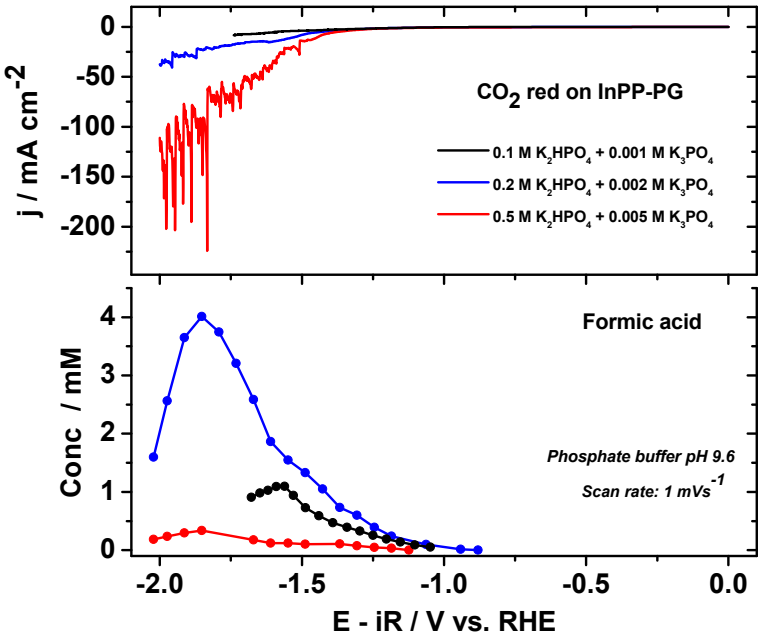

Figure B.10 CO_2 reduction on InPP-PG in phosphate buffers of pH 9.6 with different buffer capacities. Scan rate: 1 mV s^{-1}.

B.9 References

[1] G. G. Wildgoose, P. Abiman, R. G. Compton, *J. Mater. Chem.* **2009**, *19*, 4875–4886.

[2] X. Ji, C. E. Banks, A. Crossley, R. G. Compton, *ChemPhysChem* **2006**, *7*, 1337–1344.

[3] C. A. Thorogood, G. G. Wildgoose, A. Crossley, R. M. J. Jacobs, J. H. Jones, R. G. Compton, *Chem. Mater.* **2007**, *19*, 4964–4974.

[4] C. A. Thorogood, G. G. Wildgoose, J. H. Jones, R. G. Compton, *New J. Chem.* **2007**, *31*, 958–965.